The determination of creep and relaxation functions from a single experiment

A. Nikonov

Center for Experimental Mechanics, University of Ljubljana, Ljubljana, Slovenia

A. R. Davies

Institute of Mathematical and Physical Sciences, University of Wales, Aberystwyth, United Kingdom

I. Emri[a)]

Center for Experimental Mechanics, University of Ljubljana, Ljubljana, Slovenia

(Received 7 January 2005; final revision received 26 July 2005)

Synopsis

The creep compliance and relaxation functions used in characterizing the mechanical response of linear viscoelastic solids are traditionally found by conducting two separate experiments. Alternatively, one of the functions may be determined from a single experiment while the other is obtained through interconversion. All direct interconversion methods, however, require the solution of an ill-posed problem. The goal of this paper is to present the theoretical framework for developing a new apparatus, based on "spring loading," which facilitates the determination of both creep and relaxation functions from a single experiment. There is no need for interconversion. Questions of stability with respect to the measured data are discussed and a stable numerical algorithm is presented. © *2005 The Society of Rheology.* [DOI: 10.1122/1.2072027]

I. INTRODUCTION

The creep compliance and relaxation functions used in characterizing the mechanical response of linear viscoelastic materials are traditionally found by conducting two separate experiments, e.g., Ferry (1980). Alternatively, one of the functions may be determined from a single experiment while the other is obtained through interconversion [Tschoegl (1989)]. All direct interconversion methods, however, require the solution of an ill-posed problem. The standard approach is to solve a Volterra integral equation of the first kind [Hopkins and Hamming (1957); Knoff and Hopkins (1972); Mead (1994)]. Knoff and Hopkins appear to be the first to note that the conversion from creep compliance to relaxation is more unstable than the conversion from relaxation to creep (at least for viscoelastic solids). In the former case they advocate transforming the first kind

[a)]Author to whom correspondence should be addressed; electronic mail: ie@fs.uni-lj.si

Volterra equation to a second kind equation, for which their algorithm is more stable. A rigorous analysis of the benefits of this type of approach is beyond the scope of our paper, but we refer interested readers to the review of Baker (2000).

An alternative algebraic approach is possible if the material is modeled by a finite number of viscoelastic elements [Gross (1953); Park and Schapery (1999)]. However this does not remove the ill-posedness of the underlying problem [Tschoegl and Emri (1992)]. In the algebraic approach it can be shown that the degree of instability grows exponentially with the number of elements in the model. A small number of elements is, in effect, a coarse regularization. The degree of instability also depends on the distribution of the discrete relaxation (or retardation) times. These remarks are discussed further in the Appendix.

In this paper we determine both creep and relaxation functions without recourse to interconversion. The goal of the paper is to present the theoretical framework for developing a new apparatus, based on "spring loading," which facilitates the determination of both creep and relaxation functions from a single experiment. The general theory is developed in Sec. II of the paper. It will be shown that there is no need for interconversion. Moreover, the integral equations which are solved are effectively Volterra equations of the second kind. Such problems are well-posed and stable in response to errors in the data [Baker (2000)], although care must be taken to address inherent instabilities in the data.

The proposed apparatus consists of a viscoelastic bar connected in series to a Hookean spring which will be called "the load spring." This spring, initially deformed by a constant tensile deformation, will impose a force upon the bar, causing its time-dependent elongation. As the bar elongates the deformation of the load spring diminishes, causing a decrease in the force acting upon the bar. If the viscoelastic bar is made of rheodictic[1] material, as time passes, the deformation of the spring will become zero, and the length of the bar, will be increased by the initial deformation of the spring. On the other hand, if the tested material is arrheodictic,[1] the deformation of the spring will diminish to a certain equilibrium value, defined by the equilibrium modulus of the tested material. The length of the bar will be, at the same time, increased by the difference between the initial and the remaining deformation of the spring.

For convenience we discuss the response of the bar loaded in the uniaxial direction. Generalization to the loading in shear is straight forward. The key issue which enables the simultaneous determination of creep and relaxation functions is the fact that the force on the bar is related linearly to the deformation of the bar. (This is valid at all times provided the elastic limit of the load spring is not exceeded.) Within the linear viscoelastic regime the force is related to the creep function by an integrodifferential equation, while the deformation of the bar is related to the relaxation function by an equation of identical form. Measurement of force over a period of time therefore yields an inverse problem for creep, while measurement of deformation yields an identical inverse problem for relaxation. Furthermore, it is not necessary to measure both force and deformation, since one may deduced linearly from the other.

The inverse problems for creep and relaxation may be solved analytically by means of Laplace transforms. Closed form solutions are given in Sec. III of the paper. In practice, however, a numerical approach is more direct since only discrete time measurements of force and deformation can be made. In Sec. IV we present a stable numerical algorithm

[1]A material is said to be rheodictic if it is capable of showing steady-state flow, and is arrheodictic otherwise [Tschoegl (1989), p. 93].

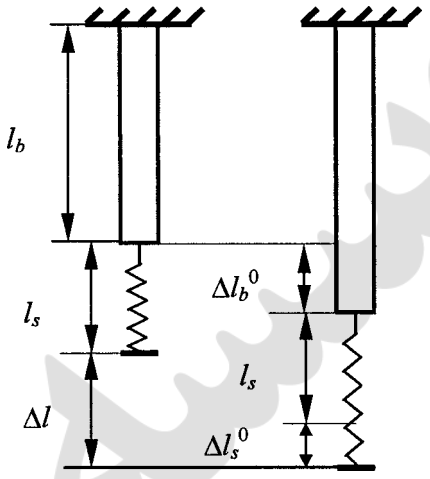

FIG. 1. A viscoelastic bar loaded instantaneously with a spring.

for solving for creep and relaxation, and demonstrate its validity by comparing numerical results with the analytical solutions obtained when the bar is represented by a three-element generalized Kelvin-Voight model.

II. GENERAL THEORY

A. Force and deformation under spring-loading

Consider a bar and load spring of lengths l_b and l_s, respectively, connected in series, as shown in Fig. 1. Let A_b be the cross section of the bar and k_s is the stiffness of the spring. Let the uniaxial linear viscoelastic behavior of the material be given with the relaxation function $E(t)$, and the creep compliance function, $D(t)$, where

$$E(t) = E_\infty + \int_0^\infty H(\tau)\exp(-t/\tau)\frac{d\tau}{\tau}, \tag{1}$$

$$D(t) = D_0 + \int_0^\infty L(\lambda)[1-\exp(-t/\lambda)]\frac{d\lambda}{\lambda}. \tag{2}$$

Here E_∞ is the equilibrium modulus, D_0 is the instantaneous elastic compliance, $H(\tau)$ is the relaxation spectrum, $L(\lambda)$ is the retardation spectrum, while τ and λ are relaxation and retardation times, respectively.

At time $t=0$ the lower end of the spring is instantly (as a step function) displaced through a distance Δl, as shown in Fig. 1. The lower end of the spring is thereafter kept in a fixed position. Due to the applied load the viscoelastic bar will elastically deform to an initial extension Δl_b^0, leaving the initial deformation of the spring to be Δl_s^0. As time progresses the viscoelastic bar will elongate due to the applied load, and the initial deformation of the spring will decrease. This will, in return, decrease the force acting upon the bar (the specimen). The tension in the spring, $F_s(t)$, and the force applied to the bar, $F_b(t)$, are equal because the spring and the bar are connected in series. In this analysis the weight of the bar and the spring will be neglected.

Let $\Delta l_b(t)$ and $\Delta l_s(t)$ denote the deformation of the bar and spring at any time t, respectively.

As the elongation of the viscoelastic specimen increases, the deformation of the spring will decrease such that the sum of the two is at any time equal to the initial (constant) displacement

$$\Delta l_b(t) + \Delta l_s(t) = \Delta l.$$

The deformed spring is acting on the viscoelastic bar with the force proportional to its extension. Consequently

$$F_b(t) = F_s(t) = k_s \cdot \Delta l_s(t) = k_s \cdot [\Delta l - \Delta l_b(t)]. \tag{3}$$

The stress in the bar, which is proportional to $F_b(t)$, and the deformation of the bar, are related through the relaxation function by the Volterra integral equation

$$F_b(t) = \frac{A_b}{l_b}\int_0^t E(t-\xi)\frac{d}{d\xi}[\Delta l_b(\xi)]d\xi + \frac{A_0}{l_b}\Delta l_b^0 E(t). \tag{4}$$

The stress and deformation are also related through the creep function by the equation

$$\Delta l_b(t) = \frac{l_b}{A_b}\int_0^t D(t-\xi)\frac{d}{d\xi}[F_b(\xi)]d\xi + \frac{l_b}{A_b}F_b(0)D(t). \tag{5}$$

From Eqs. (3) and (4) we may deduce

$$\Delta l_b(t) + \frac{A_b}{k_s l_b}\left\{\int_0^t E(t-\xi)\frac{d}{d\xi}[\Delta l_b(\xi)]d\xi + \Delta l_b^0 E(t)\right\} = \Delta l, \tag{6}$$

while from Eqs. (3) and (5) we obtain similarly

$$F_b(t) + \frac{k_s l_b}{A_b}\left\{\int_0^t D(t-\xi)\frac{d}{d\xi}[F_b(\xi)]d\xi + F_b(0)D(t)\right\} = k_s\Delta l. \tag{7}$$

Equations (6) and (7) are the two key equations in the analysis. Equation (6) gives deformation in terms of the relaxation function only, while Eq. (7) gives the force in terms of the creep function only.

If the deformation of the bar is measured, then Eq. (6) may be solved to yield the relaxation function $E(t)$. This is a well-posed inverse problem since Eq. (6) is a Volterra integral equation of the second kind. (See, however, Sec. II B.) Similarly, if the force is measured, then Eq. (7) may be solved to yield the creep function $D(t)$.

It is not difficult to see that, using Eq. (3), Eq. (6) may be rewritten so as to give force in terms of relaxation, while Eq. (7) may be rewritten so as to give deformation in terms of creep. Thus both material functions may be obtained directly from the deformation only, or both from the force. The two inverse problems may be solved simultaneously (that is, in parallel), or sequentially.

B. Consistency, well-posedness and ill-posedness

We begin by writing down the four basic equations which relate the force, deformation, creep, and relaxation functions to each other

$$\Delta l_b(t) + \frac{A_b}{k_s l_b}\left\{\int_0^t E(t-\xi)\frac{d}{d\xi}[\Delta l_b(\xi)]d\xi + \Delta l_b^0 E(t)\right\} = \Delta l, \tag{8a}$$

$$F_b(t) + \frac{k_s l_b}{A_b}\left\{\int_0^t D(t-\xi)\frac{d}{d\xi}[F_b(\xi)]d\xi + F_b(0)D(t)\right\} = k_s \Delta l, \tag{8b}$$

$$F_b(t) = k_s[\Delta l - \Delta l_b(t)], \tag{8c}$$

$$\int_0^t D(t-\xi)E(\xi)d\xi = t. \tag{8d}$$

We reiterate the method we have outlined to determine both creep and relaxation functions:

Step 1. Measure the deformation $\Delta l_b(t)$ of the bar over a range of time.

Step 2. Calculate the force on the bar $F_b(t)$ from (8c).

Step 3. Solve the inverse problem (8a) for the relaxation function $E(t)$ over the time range of the experiment, and either simultaneously or sequentially solve the inverse problem (8b) for the creep function $D(t)$ over the same time range.

A fundamental strength of the earlier method is that the functions $E(t)$ and $D(t)$ so determined will automatically satisfy the interconversion condition.

The above result is a consequence of the following:

Consistency theorem. *Any three equations from the set* [(8a)–(8d)] *imply the fourth equation.*

The proof of this theorem by means of Laplace transforms is elementary. We show only that Eqs. (8a)–(8c) imply Eq. (8d), since the proofs of the other permutations are similar. The Laplace transforms of Eqs. (8a)–(8c) may be written (in obvious notation)

$$\overline{\Delta l}_b(s) + \frac{A_b}{k_s l_b}\bar{E}(s)s\overline{\Delta l}_b(s) = \frac{\Delta l}{s}, \tag{9a}$$

$$\bar{F}_b(s) + \frac{k_s l_b}{A_b}\bar{D}(s)s\bar{F}_b(s) = \frac{k_s \Delta l}{s}, \tag{9b}$$

and

$$\bar{F}_b(s) = k_s\left[\frac{\Delta l}{s} - \overline{\Delta l}_b(s)\right]. \tag{9c}$$

Eliminating the two variables $\overline{\Delta l}_b$ and $\bar{F}_b$ between these three equations immediately yields

$$\bar{E}(s)\cdot\bar{D}(s) = \frac{1}{s^2}, \tag{9d}$$

which is the Laplace transform of (8d). ▲

Equations (8a) and (8b) are Volterra integral equations of the second kind for $E(t)$ and $D(t)$, respectively. This makes the determination of $E(t)$ and $D(t)$ stable with respect to the data. On the other hand, Eq. (8d) is a Volterra integral equation of the first kind, which makes the interconversion from $E(t)$ to $D(t)$, and vice-versa, an unstable process. At first sight it would appear that an ill-posed interconversion problem has been circumvented by determining both $E(t)$ and $D(t)$ together by solving two well-posed problems. This is technically true, but the instability has been transferred to the data. The kernel functions (part of the data) in (8a) and (8b) are derivatives of the measured quantities $\Delta l_b(t)$ and $F_b(t)$.

Differentiation is also an ill-posed process, and the degree of ill-posedness in differentiation is exactly equivalent to the degree of ill-posedness of the interconversion problem (8d) when the initial values $E(0)$ and $D(0)$ are nonzero.

Notwithstanding these remarks there are distinct advantages in determining $E(t)$ and $D(t)$ together as in the method proposed. First there is a reduction in the time required in experimentation: a single experiment takes half the time of two. Second, the linear constraint (8c) may be used to reduce the level of experimental noise in measurements of both force and deformation, using standard statistical regression methods. Third, as is shown in Sec. IV below, it is possible to devise a simple numerical algorithm for both Eqs. (8a) and (8d) which is stable with respect to the measured data $\Delta l_b(t)$.

C. Analysis of limiting cases

By observing Fig. 1 it can be easily seen that when the stiffness of the spring approaches infinity the spring-loading experiment becomes the relaxation experiment (the stiffness of the spring essentially represents the stiffness of the load cell). In this case Eq. (8a) reduces to

$$\Delta l_b(t) = \Delta l = \text{const}.$$

Hence, there will be no change in deformation. At the same time Eq. (8b) becomes

$$\frac{l_b}{A_b}\left\{\int_0^t D(t-\xi)\frac{d}{d\xi}[F_b(\xi)]d\xi + F_b(0)D(t)\right\} = \Delta l,$$

which is equivalent to Eq. (8d) provided

$$F_b(t) = \frac{A_b \Delta l}{l_b} E(t).$$

Hence, the stress in the bar relaxes in proportion to the relaxation function.

On the other hand, when the stiffness of the spring approaches zero the spring-loading experiment loses its meaning, except if we assume that the initial elongation, Δl, is simultaneously increased such that the force acting upon the specimen remains constant, i.e., $\Delta l k_s = \text{const}$.

With this additional assumption the spring-loading experiment becomes the creep experiment. Equation (8a) becomes

$$\frac{A_b}{(\Delta l k_s) l_b}\left\{\int_0^t E(t-\xi)\frac{d}{d\xi}[\Delta l_b(\xi)]d\xi + \Delta l_b^0 E(t)\right\} = 1,$$

which is again equivalent to (8d) provided

$$\Delta l_b(t) = \frac{(\Delta l k_s) l_b}{A_b} D(t).$$

From these analyses one may immediately conclude:

- The usage of a soft spring instead of a *dead-load* should be avoided in creep experiments. This is because the load applied via a spring is not constant, but reduces with time. This introduces an error into the measurement of creep. The error can be made small only if the initial extension of the spring is made very large relative to the deformation of the specimen.

- Conversely, if the initial deformation of the spring is kept constant, and the stiffness of the spring is small the prediction of the strain has an "inherent weakness," i.e., the error of the strain prediction will significantly increase as the stiffness of the spring decreases.

D. Optimal choice of spring constant

It is important to provide some insight into the optimal value of the spring constant to get the "best" data for $E(t)$ and $D(t)$ in one experiment. It should be evident from the analysis in Sec. II C earlier that the larger the spring constant, the more the relaxation process dominates the creep process, whereas the smaller the spring constant, the more the creep process dominates the relaxation process. To be quantitative, we rewrite Eq. (3) in the form $F_b(t)+k_s\cdot\Delta l_b(t)=k_s\cdot\Delta l$.

The first term on the left-hand side represents the contribution of the relaxation process under varying deformation, while the second term on the left represents the creep process under varying load. The stiffness of the spring should be selected such that the mean values over all times of the two contributions on the left hand side should have equal weight. However, the solution of this problem is a complex issue.

III. CLOSED FORM SOLUTIONS FOR THE GENERALIZED KELVIN-VOIGHT (GKV) MODEL

Analytical and closed form solutions for deformation and force in the bar as functions of time will now be derived in the simple case where the bar is represented by Kelvin-Voight elements together with a spring, all in series, the so-called GKV model [Tschoegl (1989)]. The spring in the GKV model contributes to the viscoelastic response of the bar, and should not be confused with the load-spring. For demonstration purposes it is enough to include only 3 kV elements: the general case of N elements can easily be inferred from the analysis. The relaxation function in (1) may then be written as

$$E(t) = E_\infty + E_1 e^{-t/\tau_1} + E_2 e^{-t/\tau_2} + E_3 e^{-t/\tau_3}, \tag{10}$$

where $\{E_i, \tau_i\}_{i=1}^3$ represents the discrete spectrum of elastic moduli, E_i, and relaxation times τ_i. This GKV model has seven parameters.

The corresponding creep function, with discrete retardation spectrum $\{D_i, \lambda_i\}_{i=1}^3$,

$$D(t) = D_0 + D_1(1 - e^{-t/\lambda_1}) + D_2(1 - e^{-t/\lambda_2}) + D_3(1 - e^{-t/\lambda_3}), \tag{11}$$

also has seven parameters, which may be found by inverting the integral Eq. (8d). A simple way of doing this is provided by the consistency theorem of Sec. II B. Details are given in the Appendix. Defining

$$D_\infty = D_0 + D_1 + D_2 + D_3 \tag{12}$$

and

$$E_0 = E_\infty + E_1 + E_2 + E_3, \tag{13}$$

it is easily shown that

$$D_0 = \frac{1}{E_0} \text{ and } D_\infty = \frac{1}{E_\infty}. \tag{14}$$

Table I contains an example of a discrete three-mode relaxation spectrum and its corresponding three-mode retardation spectrum.

TABLE I. Relaxation and corresponding retardation spectra.

i	E_i	τ_i	D_i	λ_i
0	10.0		0.1	
1	1.0	0.1	0.0092	0.1101
2	7.0	1.0	0.1105	3.0115
3	1.0	5.0	0.7803	15.0784
∞	1.0		1.0	

The corresponding creep and relaxation functions are shown in Fig. 2.

The deformation of the bar at time t, $\Delta l_b(t)$, is given by Eq. (8a). Writing $\alpha = A_b / l_b k_s h$, this becomes

$$\Delta l_b(t) + \alpha \int_0^t E(t-\xi) d\dot{l}_b(\xi) d\xi + \alpha \Delta l_b^0 E(t) = \Delta l, \tag{15}$$

from which the Laplace transform of the deformation is found to be

$$\overline{\Delta l}_b(s) = \frac{\Delta l}{s[1 + \delta s \bar{E}(s)]}. \tag{16}$$

For the seven parameter model, the right side of Eq. (16) may be written in the form

$$\frac{\Delta l}{(1+\alpha E_0)\tau_1\tau_2\tau_3} \cdot \frac{(1+\tau_1 s)(1+\tau_2 s)(1+\tau_3 s)}{s(s^3 + As^2 + Bs + C)}, \tag{17}$$

where the constants A, B, and C are given by

$$A = \left(\frac{1}{\tau_1} + \frac{1}{\tau_2} + \frac{1}{\tau_3}\right) - \frac{\alpha}{1+\alpha E_0}\left(\frac{E_1}{\tau_1} + \frac{E_2}{\tau_2} + \frac{E_3}{\tau_3}\right),$$

$$B = \left(\frac{1}{\tau_1\tau_2} + \frac{1}{\tau_2\tau_3} + \frac{1}{\tau_3\tau_1}\right) - \frac{\alpha}{1+\alpha E_0}\left[\frac{E_1}{\tau_1}\left(\frac{1}{\tau_2} + \frac{1}{\tau_3}\right) + \frac{E_2}{\tau_2}\left(\frac{1}{\tau_3} + \frac{1}{\tau_1}\right) + \frac{E_3}{\tau_3}\left(\frac{1}{\tau_1} + \frac{1}{\tau_2}\right)\right],$$

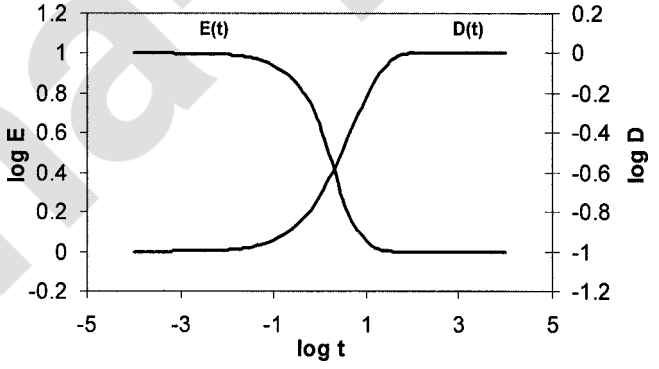

FIG. 2. Creep and relaxation curves for the parameters in Table I.

$$C = \frac{1 + \alpha E_\infty}{1 + \alpha E_0} \cdot \frac{1}{\tau_1 \tau_2 \tau_3}. \tag{18}$$

The inverse Laplace transform of Eq. (16) may then be found in terms of the three roots, $-a$, $-b$, and $-c$, of the cubic equation

$$(s + a)(s + b)(s + c) \equiv s^3 + As^2 + Bs + C = 0. \tag{19}$$

Assuming these roots are distinct, it follows that the deformation in the bar takes the form

$$\Delta l_b(t) = \Delta l_\infty - [\Delta l_1 e^{-at} + \Delta l_2 e^{-bt} + \Delta l_3 e^{-ct}] = \Delta l_0 + \Delta l_1(1 - e^{-at}) + \Delta l_2(1 - e^{-bt}) + \Delta l_3(1 - e^{-ct}). \tag{20}$$

The coefficients are best simplified using the identity

$$\tau_1 \tau_2 \tau_3 abc = \frac{1 + \alpha E_\infty}{1 + \alpha E_0},$$

and may be written

$$\Delta l_0 = \frac{\Delta l}{1 + \alpha E_0}, \quad \Delta l_\infty = \frac{\Delta l}{1 + \alpha E_\infty},$$

$$\Delta l_1 = \Delta l_\infty (1 - \tau_1 a)(1 - \tau_2 a)(1 - \tau_3 a) \frac{bc}{(a - b)(1 - c)},$$

$$\Delta l_2 = \Delta l_\infty (1 - \tau_1 b)(1 - \tau_2 b)(1 - \tau_3 b) \frac{ca}{(b - c)(b - a)},$$

$$\Delta l_3 = \Delta l_\infty (1 - \tau_1 c)(1 - \tau_2 c)(1 - \tau_3 c) \frac{ab}{(c - a)(c - b)}. \tag{21}$$

Starting from the creep function (11), in exactly the same way as before, Eq. (8b) may be solved to give the force on the bar. This takes the form

$$F_b(t) = F_\infty + F_1 e^{-at} + F_2 e^{-bt} + F_3 e^{-ct} = F_0 - F_1(1 - e^{-at}) - F_2(1 - e^{-bt}) - F_3(1 - e^{-ct}), \tag{22}$$

where a, b, and c are the same (reciprocal time) constants as for the deformation in (20). The other constants in (22) are given by

$$F_0 = \frac{\alpha k_s \Delta l}{\alpha + D_0} = \left(\frac{A_b}{l_b} E_0\right) \Delta l_0, \quad F_\infty = \frac{\alpha k_s \Delta l}{\alpha + D_\infty} = \left(\frac{A_b}{l_b} E_\infty\right) \Delta l_\infty,$$

$$F_1 = -F_\infty (1 - \lambda_1 a)(1 - \lambda_2 a)(1 - \lambda_3 a) \frac{bc}{(a - b)(a - c)},$$

$$F_2 = -F_\infty (1 - \lambda_1 b)(1 - \lambda_2 b)(1 - \lambda_3 b) \frac{ca}{(b - c)(b - a)},$$

TABLE II. Constants A, B, C, a, b, c with $\alpha=1$.

A	9.6364
B	4.4182
C	0.3636
a	0.1070
b	0.3711
c	9.1583

$$F_3 = -F_\infty(1-\lambda_1 c)(1-\lambda_2 c)(1-\lambda_3 c)\frac{ab}{(c-a)(c-b)}. \tag{23}$$

That the decay rates for the force in Eq. (22) are the same as the decay rates for the deformation in Eq. (20) should be no surprise, since force and deformation are related linearly by Eq. (8c). Physically this is a consequence of the fact that there is no time-dependent forcing term to induce a time-lag between stress and strain.

This behavior is illustrated using the relaxation and retardation spectra in Table I. We have selected the following parameters: $A_b=100$, $l_b=100$, $k_s=1$, $\Delta l=1$, and $\alpha=1$. The values of the constants in Eqs. (19) and (20) are given in Table II, while the functions $\Delta l_b(t)$ and $F_b(t)$ are shown in Fig. 3.

To produce the entries in Tables I and II correct to four places of decimal it was necessary to work with an accuracy of at least eight places of decimal.

IV. NUMERICAL METHODS

To complete the specification of the method, a numerical algorithm for solving the inverse problems associated with Eqs. (8a) and (8b) must be presented. The algorithm must be stable with respect to experimental measurements of the deformation $\Delta l_b(t)$ taken on a discrete time grid $\{t_n\}$ which in general will be nonuniform. Moreover, the accuracy of the computed values $\{E(t_n)\}$ and $\{D(t_n)\}$ should be such as to satisfy the interconversion condition (8d) at all values of t_n, to within an acceptable tolerance. In other words, the consistency theorem must be satisfied numerically to within a prescribed accuracy.

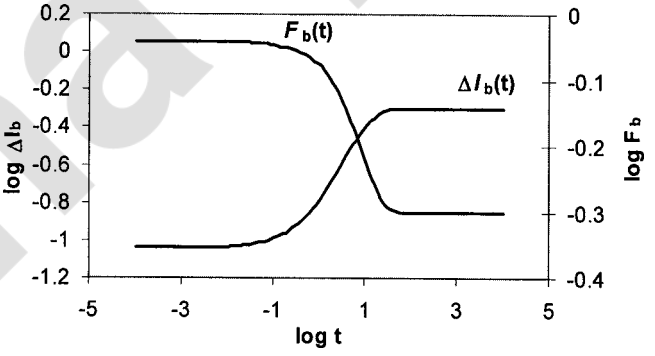

FIG. 3. Elongation and force in the bar.

A. A stable algorithm for the relaxation modulus $E(t)$ and creep compliance $D(t)$

Equation (8a) represents an *inverse problem* for determining the relaxation function from measurements of deformation, while Eq. (8b) represents an inverse problem for determining the creep compliance function from measurements of force. Both these equations, however, may be written in the form of *direct problems*. Thus (8a) may be rewritten in the form

$$E(t) - \frac{1}{\Delta l_b(0)} \int_0^t E(\xi) \frac{d\Delta l_b(t-\xi)}{d\xi} d\xi = \frac{\Delta l - \Delta l_b(t)}{\alpha \Delta l_b(0)}. \tag{24}$$

The modulus $E(t)$ on a discrete grid may be obtained iteratively using the finite-difference integration method first introduced by Lee and Rogers (1963). However, there is an additional source term in Eq. (24) which does not arise in the Volterra integral equations solved by Lee and Rogers. Although it is a trivial matter to include this additional source term numerically, nevertheless, it changes the stability criterion in Lee and Rogers original work. At $t=0$, $E(0)$ takes the value

$$E(0) = \frac{1}{\alpha}\left[\frac{\Delta l}{\Delta l_b(0)} - 1\right]. \tag{25}$$

whereas at subsequent times $t=t_n$ we may solve Eq. (24) using the iteration

$$E(t_n) = \frac{2\Delta l - 2\Delta l_b(t_n) + \alpha E(t_{n-1})[\Delta l_b^0 - \Delta l_b(t_n - t_{n-1})] + \alpha \sum_{i=1}^{n-1} [E(t_i) + E(t_{i-1})][\Delta l_b(t_n - t_i) - \Delta l_b(t_n - t_{i-1})]}{\alpha[\Delta l_b^0 + \Delta l_b(t_n - t_{n-1})]}. \tag{26}$$

The denominator in Eq. (26) is of a different form than that encountered by Lee and Rogers. The criterion for stability of the iterative scheme is

$$\left| \frac{\Delta l_b^0 - \Delta l_b(t_n - t_{n-2})}{\Delta l_b^0 + \Delta l_b(t_n - t_{n-1})} \right| \leqslant 1. \tag{27}$$

It may be shown that the stability criterion is satisfied for all finite positive values of the parameter α, provided the time step is not greater than $2\Delta l_0/(\Delta l_b)$. This is the same as saying that the stability criterion is satisfied for all finite positive values of the spring constant k_s. The proof makes use of the *monotonicity* of the deformation $\Delta l_b(t)$, which is an important feature for stability as pointed out by Hopkins and Hamming (1957).

Equation (8b) may be solved in exactly the same way for the creep compliance $D(t)$. The initial value is given by

$$D(0) = \alpha\left[\frac{k_s \Delta l}{F_b(0)} - 1\right], \tag{28}$$

and successive values are found iteratively from

$$D(t_n) = \frac{2\alpha k_s \Delta l - 2\alpha F_b(t_n) + D(t_{n-1})[F_b(0) - F_b(t_n - t_{n-1})] + \sum_{i=1}^{n-1} [D(t_i) + D(t_{i-1})][F_b(t_n - t_i) - F_b(t_n - t_{i-1})]}{[F_b(0) + F_b(t_n - t_{n-1})]}. \tag{29}$$

The stability criterion for the iteration (29) is

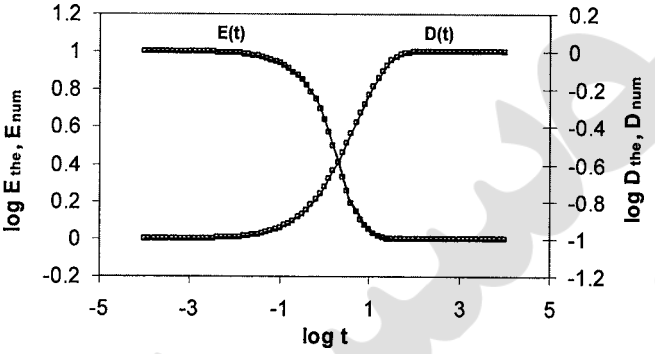

FIG. 4. Numerical and analytic curves for $E(t)$ and $D(t)$ compared.

$$\left| \frac{F_b(0) - F_b(t_n - t_{n-2})}{F_b(0) + F_b(t_n - t_{n-1})} \right| \leqslant 1, \tag{30}$$

which is valid for all positive values of α, independent of time-step. Since the ratios in (27) and (30) are both functions of the spring constant k_s, an optimal value for this constant, from the numerical viewpoint, is that which minimizes the maximum value of both ratios over all times. Again, this is not a simple matter to determine.

To demonstrate the stability and accuracy of the algorithm we perform the iterations (26) and (29) on a time grid consisting of 101 discrete times t_n which are exponentially distributed over the range $10^{-4} \leqslant t \leqslant 10^4$, or equivalently, uniform in $\log t$ in the interval $[-4, 4]$.

Exact values of $\Delta l_b(t_n)$ and $F_b(t_n)$ on the time grid are obtained from the closed form solutions (20) and (22) using the model with parameters in Tables I and II, but linear interpolation is used to find values of $\Delta l_b(t_n - t_k)$ and $F_b(t_n - t_k)$ off-grid. There are therefore no measurement errors on-grid, but there are interpolation errors off-grid. Additional numerical errors are encountered in the quadruatures by taking mean values of $E(t)$ and $D(t)$ over each time subinterval.

The numerical and analytic curves are shown in Fig. 4 and are seen to be indistinguishable from each other on the log-log scale of the diagram. The absolute errors of the numerical prediction of the relaxation modulus and creep compliance are shown in Fig. 5. Roughly speaking the greatest errors correspond to the regions of greatest slope, and in

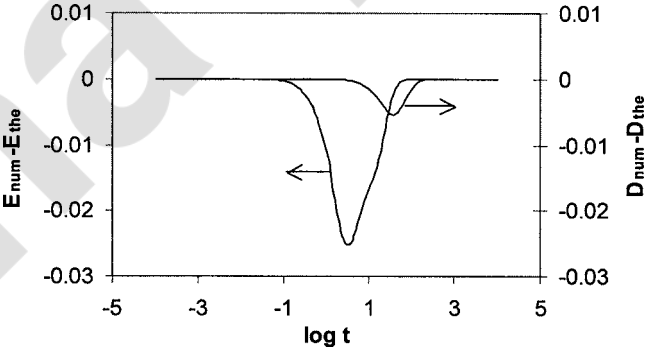

FIG. 5. Absolute errors in numerical solution of $E(t)$ and $D(t)$.

these regions the errors in predicting the relaxation function are greater than those for the creep compliance, a result which has been reported by other authors [Hopkins and Hamming (1957); Knoff and Hopkins (1972)]. The maximum relative errors are 1% in $E(t)$ and 0.6% in $D(t)$.

B. Numerical validation of the interconversion condition

From an analytic viewpoint, the creep compliance and relaxation functions obtained from Eqs. (8a) and (8b) will automatically satisfy the interconversion condition (8d). To validate the method of this paper, it must now be shown that the interconversion condition holds, to within acceptable accuracy, for numerically derived values of $E(t)$ and $D(t)$. This is by no means an easy matter since there are several sources of error in calculating the convolution integral in (8d), namely:

(a) errors of measurement and interpolation of the deformation $\Delta l_b(t)$ which contribute to data errors in (8a) and (8b);
(b) discretization errors in the Volterra solver of Sec. IV A applied to (8a) and (8b);
(c) quadrature errors in evaluating the convolution;
(d) truncation error due to lack of information close to $t=0$; and
(e) interpolation errors in evaluating off-grid values of $E(t)$ and $D(t)$.

In the absence of measurement errors in (a) it will be demonstrated below that (c) and (e) are the most dominant sources of error.

Consider, first, the two convolution integrals

$$C_1(t) = \int_0^t D(t-\xi)E(\xi)d\xi, \tag{31a}$$

$$C_2(t) = \int_0^t E(t-\xi)D(\xi)d\xi. \tag{31b}$$

Analytically, the two are equivalent, and the interconversion condition (8d) may be rewritten in the form

$$C_1(t) = C_2(t) = t.$$

When calculated numerically, however, the two convolutions will differ, in general, and it is of distinct advantage to calculate both, since a combination of the two results may be used to reduce the numerical error.

In particular let μ be a constant, and let

$$C(t) = (1-\mu)C_1(t) + \mu C_2(t). \tag{32}$$

Analytically we know that $C(t)=C_1(t)=C_2(t)$ for all values of μ. Numerically, however, the value of μ may be chosen to reduce the error in $C(t)$ *through cancellation* of the errors in $C_1(t)$ and $C_2(t)$. Such an approach can be very effective as we shall demonstrate later.

Let the two convolution integrals (31a) and (31b) be discretized using the composite trapezium rule as follows:

$$C_1(t_n) \approx \frac{1}{2}\sum_{i=1}^{n} [D(t_n - t_{i-1})E(t_{i-1}) + D(t_n - t_i)E(t_i)](t_i - t_{i-1}), \tag{33a}$$

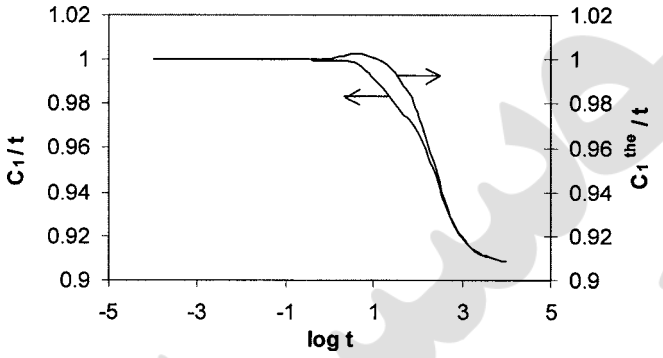

FIG. 6. Comparison of trapezium quadrature results from (33a) using exact and inexact on-grid data.

$$C_2(t_n) \approx \frac{1}{2}\sum_{i=1}^{n} [E(t_n - t_{i-1})D(t_{i-1}) + E(t_n - t_i)D(t_i)](t_i - t_{i-1}). \tag{33b}$$

Off-grid values of E and D at times $t_n - t_k$ are obtained by linear interpolation in the appropriate time subinterval.

First we show that errors resulting from the Volterra solver [source (b)] are of little significance. Using exact values of $E(t)$ and $D(t)$ on-grid obtained from Eqs. (10) and (11) with the parameters in Table I and using linear interpolation off-grid, we calculate the convolution in (33a), and denote the results by $\{C^{\text{the}}(t_n)\}$. Next we repeat the calculation in (33a), but this time using the numerical values of $E(t)$ and $D(t)$ on-grid obtained from the Volterra solver iterations (26) and (29). These results are denoted by $\{C_1(t_n)\}$. Any difference between the two sets of results will be due to errors from the Volterra solver.

The two sets of discrete convolutions, $\{C_1(t_n)\}$ and $\{C_1^{\text{the}}(t_n)\}$, computed from (33a), are plotted relative to their exact values, t, on a linear-log scale in Fig. 6.

In the range $10^{-4} \leqslant t \leqslant 1$, both convolutions are in close agreement with the exact value, t, but as t increases further to 10^4, the exact value is underpredicted by as much as 9% in each case.

It is clear from the figure, however, that it makes little difference as to whether exact or inexact data were used in the discrete convolutions, which demonstrates that the greatest errors stem from sources (c) and (e).

The same calculations are now shown for the second discrete convolution (33b). Figure 7 shows the difference between using exact and inexact data in the convolution, when compared relative to the exact value t. The difference is indistinguishable on a linear-log scale. At the larger times near 10^4, the discrete convolution (33b) overpredicts its exact value, t, by some 90%, whether exact or inexact data are used. The second formulation (33b) is therefore considerably less accurate than the first formulation (33a).

In Fig. 8 we compare, relative to the exact quadrature value t, the three quadrature estimates, $C(t)$ with a value of $\mu = 0.09$, $C_1(t)$ and $C_2(t)$, obtained from (32), (33a), and (33b), respectively. This choice of μ reduces the error in $C(t)$ to 4%. Here we must discuss, therefore, how this choice of μ is made.

From Fig. 8 we see that the larger quadrature/interpolation errors associated with (33a) and (33b) are, roughly speaking,

(i) of opposite sign; and

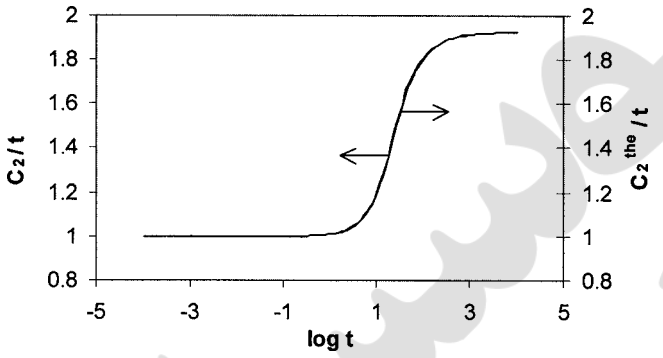

FIG. 7. Comparison of trapezium quadrature results from (35b) using exact and inexact on-grid data.

(ii) grow approximately in proportion as t increases.

Observation (i) implies that taking an average of the two estimates would reduce the error. Observation (ii) implies that the two error distributions may be described by the same (approximate) shape factor. If we denote the common shape factor by $\Xi(t)$ and choose two scalings of opposite sign, which add up to unity, we may write the errors in the form

$$C(t) - C_1(t) = \left(\frac{-\mu}{1-2\mu}\right)\Xi(t), \tag{34a}$$

$$C(t) - C_2(t) = \left(\frac{1-\mu}{1-2\mu}\right)\Xi(t), \tag{34b}$$

where μ is a constant which we choose below. Here $C(t)$ denotes the exact value of the convolution integral (31a), or (31b), whereas $C_1(t)$ and $C_2(t)$ denote numerical approximations (33a) and (33b). Eliminating the unknown shape factor $\Xi(t)$ between these two equations gives (32).

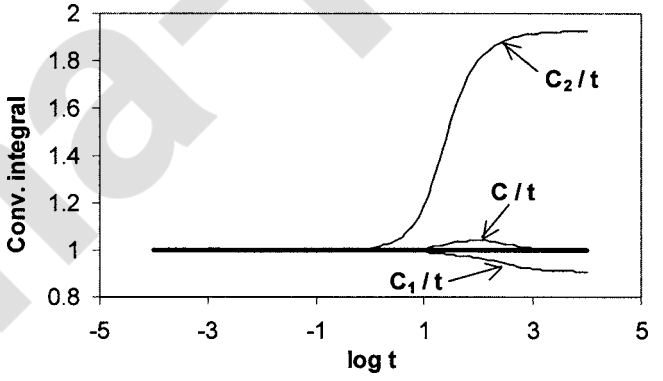

FIG. 8. Comparison of three quadrature estimates $C(t)$, $C_1(t)$, and $C_2(t)$ relative to the exact quadrature value t.

It is evident that we can make the linear combination in (32) exact, at a chosen value of t, by choosing μ appropriately. Let us force the identity $C(t^*)=t^*$ at one point $t=t^*$. This requires the following choice of μ:

$$\mu = \frac{t^* - C_1(t^*)}{C_2(t^*) - C_1(t^*)}. \tag{35}$$

If we pick the value of t^* wisely then the linear combination (32) together with the choice of μ in (35) will redistribute the errors and induce cancellations.

Since the errors are greatest at the largest time we choose $t^*=10^4$, which gives a value of $\mu \approx 0.09$. As seen from Fig. 8 the improvement in accuracy is significant, reducing a maximum error of 90% in $C_2(t)$ to only 4% in $C(t)$. The new error distribution is also very different, the maximum error now occurring at $t \approx 100$.

Of course, higher order quadrature rules and higher order interpolation could be used to reduce the convolution errors even more, but that is not the aim of this paper. It has been successfully demonstrated that, using the method proposed, both creep and relaxation functions may be determined simultaneously from a single experiment, and that they can be shown to satisfy the interconversion constraint to within an acceptable tolerance.

V. CONCLUSIONS

We have presented the theoretical framework for the simultaneous measurements of creep compliance and relaxation functions with a single spring-loading experiment. It has been shown that the proposed iterative numerical algorithm for determining both $E(t)$ and $D(t)$ is stable, and yields results that satisfy the interconversion constraint to within an acceptable tolerance.

It has been shown also that care is needed in calculating long-time discrete convolutions. Numerical errors can be significantly reduced by calculating the two estimates obtained from reversing the order of convolution, and taking an appropriate linear combination of the two estimates. This approach may be used as an alternative to increasing the number of measured data points per unit of time, when this is experimentally costly or infeasible.

All the data encountered in this work have been simulated. More sophisticated numerical methods based on spline interpolation or smoothing may be required when dealing with experimental data.

The developed mathematical framework presented here may serve as the underlying theory for new generation apparatus for the characterization of time-dependent behavior of solid polymers in the linear viscoelastic regime. However, by determining the two material functions of creep and relaxation simultaneously we can examine whether the determined functions satisfy the linear constraint (8d). If this is found not to be the case, then the material behavior is outside the linear viscoelastic regime. The experimental-computational (hybrid) approach embodied here, therefore, can be used for determining the linear-viscoelastic limit of polymeric materials.

ACKNOWLEDGMENTS

The authors would like to acknowledge many discussions with, and comments from, Robert Cvelbar, which contributed to the quality of the paper. This work was supported by the Ministry of Science, Education and Sports of the Republic of Slovenia, and in its later stages by the Joy Welch Educational Trust, UK.

APPENDIX: EXACT DETERMINATION OF THE DISCRETE RETARDATION SPECTRUM FROM THE DISCRETE RELAXATION SPECTRUM

In this Appendix we show that the retardation times $\{\lambda_k\}_{k=1}^N$ may be determined as the zeros of a polynomial of degree N, whose coefficients are functions of the relaxation spectrum $\{E_k, \tau_k\}_{k=1}^N$. This is not in itself a new result, but the algorithm we propose enables the analysis of the degree of instability in the interconversion process. We use the consistency theorem in Sec. II B which shows that the relaxation and creep functions obtained from Eqs. (8a)–(8c), given the deformation, automatically satisfy Eq. (8d). Again we give the algebra only for the case $N=3$, which is easily generalized to any value of N.

First we find the three roots, $-a$, $-b$, and $-c$, of the cubic Eq. (19). Then, substituting the expressions for $\Delta l_b(t)$ and $F_b(t)$ in (20) and (22) into (8c) and comparing coefficients of the exponential terms, we observe that the constants are related by

$$F_i = k_s \Delta l_i, \quad i = 1,2,3.$$

Hence, from (21) and (23) we find

$$(1-\lambda_1 a)(1-\lambda_2 a)(1-\lambda_3 a) = f(a),$$

$$(1-\lambda_1 b)(1-\lambda_2 b)(1-\lambda_3 b) = f(b),$$

$$(1-\lambda_1 c)(1-\lambda_2 c)(1-\lambda_3 c) = f(c),$$

where

$$f(x) = -\frac{(1-\tau_1 x)(1-\tau_2 x)(1-\tau_3 x)}{\alpha E_\infty}.$$

The moments

$$X_1 = -(\lambda_1+\lambda_2+\lambda_3),$$

$$X_2 = \lambda_1\lambda_2+\lambda_2\lambda_3+\lambda_3\lambda_1,$$

$$X_3 = -\lambda_1\lambda_2\lambda_3,$$

may then be calculated by solving the matrix system

$$\begin{pmatrix} a & a^2 & a^3 \\ b & b^2 & b^3 \\ c & c^2 & c^3 \end{pmatrix} \begin{pmatrix} X_1 \\ X_2 \\ X_3 \end{pmatrix} = \begin{pmatrix} f(a)-1 \\ f(b)-1 \\ f(c)-1 \end{pmatrix}. \tag{A1}$$

The retardation times $\lambda_1, \lambda_2, \lambda_3$ are then given by the three roots of the equation

$$s^3 + X_1 s^2 + X_2 s + X_3 = 0.$$

This appears to be the simplest algebraic method for obtaining discrete retardation times from the relaxation spectrum in the case of the GKV model.

We have already discussed the ill-posedness of the interconversion of one spectrum to the other, which emerges since Eq. (8d) is a Volterra integral equation of the first kind. The algebraic approach does not circumvent the ill-posedness. In the case of an N-element GKV model the N retardation times $\{\lambda_k\}_{k=1}^N$ are given by the zeros of a polynomial of degree N, where the coefficients of the polynomial are simple functions of the relaxation spectrum. Although we may calculate the zeros to arbitrary accuracy using

mathematical software packages such as MAPLE, the ill-posedness of the interconversion manifests itself in the sensitivity of the zeros to very small changes in the coefficients. Thus, small changes in the relaxation spectrum lead to small changes in the coefficients which in turn lead to very large changes in one or more zeros, particularly as N increases.

A quantitative analysis of this may be made by noting that the matrices encountered in (A1) above and (A2) below are of *Vandermonde form*. The ill conditioning of such matrices is well known. Gautschi (1975a, 1975b) has shown that their condition numbers can grow exponentially with matrix order, and also how the condition number depends on node distributions (element sizes). A very useful recent survey has been given by Li (2005).

It remains to determine exactly the discrete compliances $\{D_k\}_{k=1}^3$ from the relaxation spectrum $\{E_k, \tau_k\}_{k=1}^3$. Again, the generalization to larger values of n is straightforward. Taking the Laplace transforms of Eqs. (10) and (11) we find

$$s\bar{E}(s) = E_\infty + \sum \frac{E_k \tau_k s}{1 + \tau_k s},$$

$$s\bar{D}(s) = D_\infty - \sum \frac{D_k \lambda_k s}{1 + \lambda_k s}.$$

Expanding these summations in powers of s and substituting the result in Eq. (9d) gives

$$\Big[E_\infty + \sum E_k \tau_k s\{1 - \tau_k s + (\tau_k s)^2 - \ldots\}\Big]\Big[D_\infty - \sum D_k \lambda_k s\{1 - \lambda_k s + (\lambda_k s)^2 - \ldots\}\Big] = 1.$$

Comparing powers of s on both sides of this equation yields

$$E_\infty D_\infty = 1,$$

$$-E_\infty \sum \lambda_k D_k + D_\infty \sum \tau_k E_k = 0,$$

$$E_\infty \sum \lambda_k^2 D_k - \Big(\sum \lambda_k D_k\Big)\Big(\sum \tau_k E_k\Big) - D_\infty \sum \tau_k^2 E_k = 0,$$

$$-E_\infty \sum \lambda_k^3 D_k + \Big(\sum \lambda_k^2 D_k\Big)\Big(\sum \tau_k E_k\Big) + \Big(\sum \lambda_k D_k\Big)\Big(\sum \tau_k^2 E_k\Big) + D_\infty \sum \tau_k^3 E_k = 0.$$

Hence, the compliances D_k may be obtained by solving the matrix system

$$\begin{pmatrix} \lambda_1 & \lambda_2 & \lambda_3 \\ \lambda_1^2 & \lambda_2^2 & \lambda_3^2 \\ \lambda_1^3 & \lambda_2^3 & \lambda_2^3 \end{pmatrix} \begin{pmatrix} D_1 \\ D_2 \\ D_3 \end{pmatrix} = \begin{pmatrix} \alpha_1 \\ \alpha_2 \\ \alpha_3 \end{pmatrix} \tag{A2}$$

with

$$\alpha_1 = \frac{1}{E_\infty^2} \sum \tau_k E_k,$$

$$\alpha_2 = \frac{1}{E_\infty^2} \sum \tau_k^2 E_k + \frac{1}{E_\infty}\Big(\sum \tau_k E_k\Big)\alpha_1,$$

$$\alpha_3 = \frac{1}{E_\infty^2} \sum \tau_k^2 E_k + \frac{1}{E_\infty}\Big(\sum \tau_k^2 E_k\Big)\alpha_1 + \frac{1}{E_\infty}\Big(\sum \tau_k E_k\Big)\alpha.$$

References

Baker, C. T. H., "A perspective on the numerical treatment of Volterra equations," J. Comput. Appl. Math. **125**, 217–149 (2000).

Ferry, J. D., *Viscoelastic Properties of Polymers*, 3rd ed. (Wiley, New York, 1980).

Gautschi, W., "Norm estimates for inverses of Vandermonde matrices," Numer. Math. **23**, 337–347 (1975a).

Gautschi, W., "Optimally conditioned Vandermonde matrices," Numer. Math. **24**, 1–12 (1975b).

Gross, B., *Mathematical Structure of the Theories of Viscoelasticity* (Hermann, Paris, 1953).

Hopkins, I. L., and R. W. Hamming, "On creep and relaxation," J. Appl. Phys. **28**, 906–909 (1957).

Knoff, W. F., and I. L. Hopkins, "An improved numerical interconversion for creep compliance and relaxation modulus," J. Appl. Polym. Sci. **16**, 2963–2972 (1972).

Lee, E. H., and T. G. Rogers, "Solution of viscoelastic stress analysis problems using measured creep or relaxation functions," J. Appl. Mech. **30**, 127–133 (1963).

Li, R.-C., "Asymptotically optimal lower bounds for the condition number of a real Vandermonde matrix," Technical report rc-05, Department of Mathematics, University of Kentucky, Lexington, 2005.

Mead, D. W., "Numerical interconversion of linear viscoelastic functions," J. Chromatogr., A **38**, 1769–1795 (1994).

Park, S. W., and R. A. Schapery, "Methods of interconversion between linear viscoelastic material functions. Part I—A numerical method based on Prony series," Int. J. Solids Struct. **36**, 1653–1675 (1999).

Tschoegl, N. W., *The Phenomenological Theory of Linear Viscoelastic Behavior* (Springer, Berlin, 1989).

Tschoegl, N. W., and I. Emri, "Generating line spectra from experimental responses. Part 3. Interconversion between relaxation and retardation behavior," Int. J. Polym. Mater. **18**, 117–127 (1992).